4th URSI AT-RASC, Gran Canaria, 19 – 24 May 2024

Assessing the Feasibility of Metallic-type FDM 3D Printed Antennas at K-band

Saúl S. Carvalho*(1)(2), Samuel M. Heleno(1)(2), João R. Reis(1)(2), and Rafael F.S. Caldeirinha(1)(2)
(1) Polytechnic of Leiria, Leiria, Portugal
(2) Instituto de Telecomunicações, Leiria, Portugal

Abstract

This paper explores the potential of Fused Deposition Modelling (FDM) three-dimensional (3D) printing for the cost-effective production of metallic-type antennas, particularly horn antennas aiming at K-band. The focus is on the electromagnetic (EM) performance of two 3D printable metallic materials: BASF - Ultrafuse 316L; and Formfutura - MetalFil Classic Copper. Simulations were conducted on horn antennas at 18 to 26.5 GHz, revealing that the total efficiency of the 3D printed antennas decreases almost linearly with the increase in surface roughness, impacting on the overall performance. The MetalFil Classic Copper antenna exhibits a more pronounced decrease in efficiency due to its lower electrical conductivity and increased surface roughness. The study highlights substantial cost savings with FDM printing compared to traditional manufacturing methods, e.g., metal milling, with the Ultrafuse antenna being approximately 10 times cheaper and the MetalFil antenna around 100 times cheaper than their traditional counterparts. Consequently, 3D printing is sought to be a viable solution for fast prototyping while yielding similar EM radiation efficiency compared to that of traditional milling (subtracting) techniques.

1 Introduction

Additive Manufacturing (AM), commonly known as 3D printing, emerges as a pivotal technology for producing a wide array of devices across diverse applications [1]. In contrast to conventional subtractive manufacturing methods like machining, AM offers the notable advantage of minimizing material waste. Furthermore, the availability of numerous commercially accessible machines and materials within the 3D printing realm facilitates the swift prototyping of specific components at a reduced cost [1]. However, despite these advantages, a noteworthy gap exists in material analysis. On 3D printable metals, datasheets predominantly focus on mechanical and thermal properties, overlooking electromagnetic (EM) properties such as electrical conductivity. This poses challenges for researchers seeking to incorporate these materials into devices like antennas or other radio-frequency components. In many instances, the lack of comprehensive studies on EM properties hinders the seamless integration of 3D printed materials into applications requiring a nuanced understanding of these characteristics.

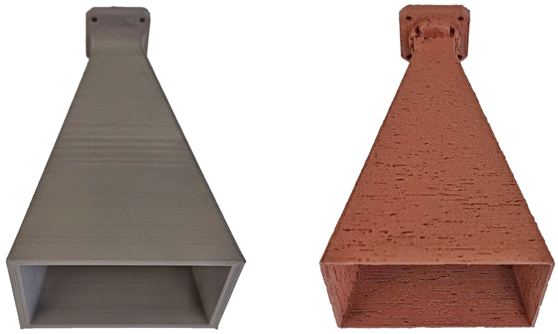

(a) **(b)**

Figure 1. 3D Printed WR-42 horn antennas: (a) Ultrafuse 316L and, (b) MetalFil Classic Copper.

Particularly in Radio Frequency applications, 3D printing methods are significantly of interest for the fabrication of antennas (Fig. 1). As reported in [1], the current state-of-the-art in 3D printed antennas encompasses a diverse range of fabrication techniques, with the following being the most common: FDM [2, 3], Stereolithography (SLA) [4, 5], and Direct Metal Laser Sintering (DMLS) [6, 7]. These techniques employ various materials in different formats, including filaments [2, 3], resins [4, 5], and powders [6, 7]. In the realm of antennas, when utilizing 3D printing, diverse designs can be implemented, creating full dielectric, full-metal, or hybrid 3D printed antennas, covering frequencies from the L-band to the G-band.

This paper aims to assess the EM performance of selected 3D printable metallic materials relevant to antenna technology. The potential application of these materials lies in the cost-effective construction of metallic antennas for various purposes. Horn antennas were chosen for evaluation due to their straightforward design and fabrication, while FDM was selected as the 3D printing method due to its widespread availability. Notably, FDM 3D printing from the connector side to the aperture side eliminates the requirement for complex build supports, resulting in reduced material waste. The paper's structure unfolds as follows: Section II provides a brief literature overview characterizing the employed materials, crucial for optimizing designs in simulations. Section III presents a qualitative analysis of the lateral surface of the samples. Section IV delves into the simulation results. Lastly, Section V comprises the key conclusions drawn from the study.

2 FDM material characterization for antenna production

For the production of the horn antennas the chosen materials were BASF - Ultrafuse 316L [8] and Formfutura - MetalFil Classic Copper [9]. To enhance the accuracy of simulations, a literature review was conducted to address potential information gaps in the material models. The summarized information is presented in Table 1. The density values in the previous table were determined for flatwise samples, aligning with the orientation in which the horns would be subsequently 3D printed. In cases where specific data was unavailable, certain values were extrapolated from comparative analyses.

The Ultrafuse filament primarily consists of 88% 316L stainless steel powder with particle sizes ranging from 2 to 17 μm, while the remaining portion consists of a thermoplastic polylactic acid (PLA) acting as a binder [10]. Before printing, the material had a relative density of 4.85 g/cm^3 [10], while post-printing density values are reported in the technical datasheet [8] as 7.80 g/cm^3, and in article [11] as 7.75 g/cm^3, with the latter being considered for the simulations performed in this work. Surface roughness measurements in [12] at a deposition angle of 90° revealed average values (R_a) of 8.38 μm and 4.84 μm at layer heights of 0.10 mm and 0.30 mm, respectively. A conversion to root mean square (RMS) terms (R_q) yielded a value of 9.31 μm. Electrical conductivity (σ) was estimated by deriving thermal conductivity (κ) data from [11], with a specified profile resembling our scenario, resulting in an estimated σ of 106.94×10^3 S/m based on a κ of 0.791 W/m·K at 30 °C.

For the MetalFil filament, the material consists of 80% copper and 20% PLA, with a reported density of 3.4 g/cm^3, as depicted in the manufacturer's datasheet [9]. However, the available technical document does not specify whether this density is before or after the printing process. Therefore, it is assumed that this value corresponds to the pre-printing state, considering its relatively low magnitude. For the simulations, considering the observed density increase of approximately 60% post-printing for the Ultrafuse 316L material, a minimum increase of 50% in density post-printing was assumed for the MetalFil material. This assumption led to a calculated density of 5.10 g/cm^3 for the MetalFil material after the printing process. The study presented in [13] describes that the resistivity (ρ) of the material is at 4×10^{-4} Ω·m, and, as such, the value of σ is 2.50×10^3 S/m.

The study in [14] presents Selective Laser Sintering (SLS) 3D printed scaffolds with stainless steel 316L powder, demonstrating a σ of 1.8×10^6 S/m. This value is several orders of magnitude higher than the value of 106.94×10^3 S/m presented for the Ultrafuse 316L filament. Additionally, information from [15] indicates that aluminum has a σ of 38×10^6 S/m, while copper has 59×10^6 S/m, the latter significantly higher than the reported value for MetalFil. These discrepancies may be attributed to several factors, notably the impurity of the metal powders used in the composite filaments and the presence of a polymeric binder, such as PLA. These factors substantially reduce the σ values in 3D printed metal composites compared to their full-metal counterparts, whether they are 3D printed or not, as was the case with the SLS steel scaffolds. Typically, metallic-type antennas like horn antennas are created with metals such as copper, aluminum, brass, or steel. Refined metals such as the aforementioned ones can cost between 0.20 to 8 €/kg while the employed filaments cost vary from 55 to 150 €/kg. While the price of the employed filaments might be several times higher than the refined metals, the difference of cost relies mostly on the process of fabrication, since the final cost of an antenna can rely on a series of investments accounting for fabrication equipment, engineering, materials, logistics and others.

Table 1. Summary of characteristics of the employed 3D printing materials (after printing), and other full metal material solutions.

AM Technique	Material (Filament)	Conductivity [S/m]	Density [g/cm^3]	RMS Surface Roughness [μm]
FDM	BASF - Ultrafuse 316L	106.94×10^3	7.75	9.31
	Formfutura - MetalFil Classic Copper	2.50×10^3	5.10	20
SLS	Stainless steel 316L	1.8×10^6	–	–
not applicable	Copper	59×10^6	–	–

3 Qualitative analysis of material samples

To accurately simulate the antennas with their designated materials, the initial step involved the creation of FDM samples. These samples were meticulously crafted into precisely shaped 10 mm cubes, for all 3D printing materials, maintaining a layer height of 0.20 mm. The manufacturing procedure was carried out using a Flashforge Creator3, highlighting the versatility of this 3D printing technology. Following fabrication, the samples underwent qualitative analysis through observation under a digital microscope, focusing on their lateral side. To enhance observation and image acquisition, a custom-fabricated light-box with uniform and diffuse lighting was utilized. Upon inspection, the surface of the reference antenna, a WR-42 Standard Gain Horn Antenna, whose body is crafted from machined aluminum, appeared very smooth, although marks from the milling process were discernible (Fig. 2a).

The Ultrafuse (Fig. 2b) sample displayed nearly flawless structures, showcasing even 0.20 mm layer raster lines and an absence of significant defects. This indicates a high compatibility and successful integration with the 3D printing process. However, the MetalFil sample (Fig. 2c) exhibited noticeable random defects, including uneven height layers in the 0.20 mm raster lines and sporadic holes on the surface. These anomalies were attributed to potential nozzle clogging during printing, likely stemming from the fact that most commercially available 3D printers were not explicitly designed for handling composite materials. Despite employing manufacturer-recommended settings, these may not be optimal for the specific 3D printer used, necessitating future minor adjustments.

In the absence of specific studies on surface roughness for

(a) **(b)** **(c)**

Figure 2. Microscope photos: (a) Aluminum machined surface of the reference antenna, (b) BASF - Ultrafuse 316L, and (c) Formfutura - MetalFil Classic Copper.

MetalFil, a qualitative approach was adopted. Acknowledging the inherent uncertainties in extracting roughness values from a single image, it is assumed that the R_q for MetalFil is approximately twice that of Ultrafuse, measured at 20 μm.

4 Horn antenna fabrication and simulation

After material characterization, horn antennas were specifically designed for the K-Band (18 to 27 GHz), aligning with the WR-42 waveguide standard (18 to 26.5 GHz) of a chosen reference antenna. Subsequently, the 3D printed models were simulated using the values provided in Table 1. Horn antennas were designed with waveguide dimensions of 10.668 mm (width) by 4.318 mm (height) and an overall length of 120 mm. All horn antenna materials were modeled as lossy metals. The wall thicknesses of the reference antenna and copper antenna were set as 1 mm, while the Ultrafuse was increased to 2 mm. In the case of the latter, this adjustment aimed to enhance the hardness and stability of the printed part.

All simulations were carried out using CST Microwave Studio, covering both the reference antenna and the FDM printed antennas. The realized gain over the frequency obtained for the three antennas is illustrated in Fig. 3a, indicating values ranging from 18.57 to 21.31 dBi, 16.61 to 19.14 dBi, and 17.89 to 20.52 dBi, within the bandwidth defined between 18 to 26.5 GHz for the reference, MetalFil, and Ultrafuse antennas, respectively. This clearly demonstrates the impact that the selected materials have in realized gain performance. The return loss is depicted in Fig. 3b, demonstrating a good match for all three cases, although the aluminum antenna exhibits deeper resonance nulls throughout the frequency band.

Antenna radiation patterns for all simulated antennas are presented at 22 GHz in Fig. 3c and Fig. 3d, for azimuth and elevation, respectively. The azimuth and elevation patterns are similar for all three cases, with a slight difference for the MetalFil antenna. Azimuth sidelobe levels (SLL) for the reference, Ultrafuse, and MetalFil antennas were -29.1 dB, -29.5 dB, and -29.4 dB, respectively. The azimuth half-power beamwidth (HPBW) was 17.8°, 17.9°, and 17.9° for the reference, Ultrafuse, and MetalFil antennas. For elevation, SLL was -11.5 dB for the reference and Ultrafuse antennas, and -11.0 dB for the MetalFil. The elevation

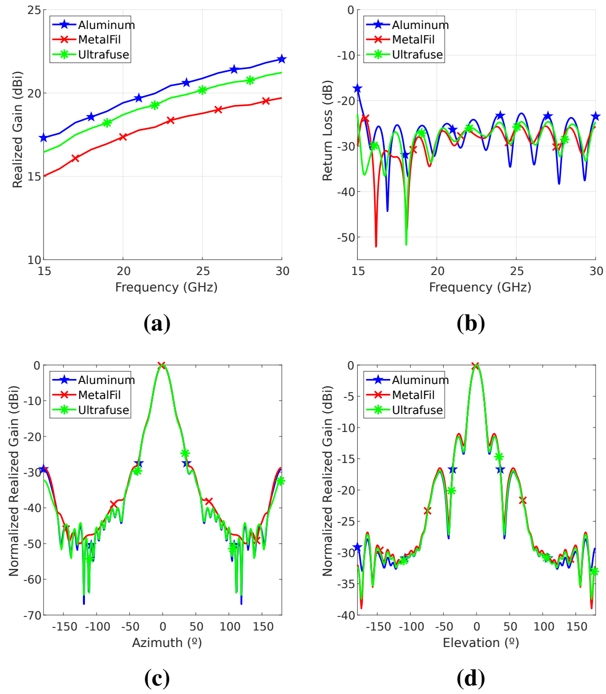

Figure 3. Simulated results for the MetaFil, Ultrafuse and reference antennas: (a) realized gain, (b) return loss, (c) azimuth, and (d) elevation radiation patterns at 22 GHz.

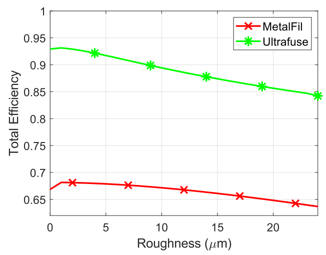

Figure 4. Antenna total efficiency as a function of surface roughness at 22 GHz.

HPBW was 17.3° for the reference and MetalFil antennas, and 17.2° for the Ultrafuse. At 22 GHz, total efficiency was 98.2% for the reference antenna, 89.7% for the Ultrafuse antenna, and 64.8% for the MetalFil antenna.

A study of the total efficiency as a function of R_q was conducted for all the simulated 3D printed antennas at a frequency of 22 GHz, as depicted in Fig. 4. This analysis aimed to observe the extent of the impact of surface roughness on the performance of each antenna. As surface roughness increases, the efficiency of the antenna decreases almost linearly. For the same surface roughness value, e.g. 5 μm, the efficiency values are 91.7% and 67.9% for the Ultrafuse and MetalFil antennas, respectively. This difference of approximately 24% is due to the properties of the materials themselves. In this case, since both densities are very similar, the difference could be mainly attributed to the lower σ in the MetalFil antenna. This can also explain the lower gain presented in Fig. 3a. Lastly, the horn antennas were manufactured (Fig. 1) using a Flashforge Creator3, employing a layer thickness of 0.20 mm and following the manufacturer's recommended fabrication settings [8, 9].

5 Conclusions

In this study, simulations provided insights into the impact of surface roughness and σ on the 3D printing of horn antennas, evaluating their feasibility for fabrication using the FDM technique. The findings revealed that total efficiency decreases almost linearly with increasing surface roughness, subsequently affecting realized gain. This trend could be attributed to the rise in resistance due to the increase of effective area, which then increases the absorption of radiation through the antenna structure. With an increase in surface roughness, the scattering of EM waves also increases, redirecting the radiated energy to undesired directions. Additionally, it was observed that a decrease in σ results in a drastic reduction in efficiency, as more power is dissipated as heat in the antenna structure. Since the material becomes less capable of reflecting EM waves, it also increasingly absorbs more radiation. This highlights the importance of using both highly conductive and smooth materials in the fabrication of metal-type antennas via 3D printing techniques, such as 3D printed horn antennas.

Furthermore, the estimated cost for fabricating both antennas through FDM, considering the materials, power consumption and fabrication process, the Ultrafuse antenna costs approximately 10 times less than traditional machining fabrication. In contrast, the MetalFil antenna is estimated to be around 100 times less expensive than machining, at an expense of lower performance. Ongoing efforts involve the production of additional horn antennas using alternative 3D printing materials and AM techniques. Subsequently, EM measurements will be conducted in an anechoic chamber for all the 3D printed horn antennas, aiming to evaluate their performance and make comparisons with the simulated models. For future endeavors in the characterization of metallic materials, it is recommended to utilize appropriate equipment for assessing σ and surface roughness, thus optimizing the designs during simulation stage.

6 Acknowledgments

This work is partially funded by Portugal PRR - Plano de Recuperação e Resiliência (The Recovery and Resilience Plan), under project INOV.AM and when applicable, by EU funds under the project 2020-2023- UIDB/50008/2020 e UIDP/50008/2020. The authors acknowledge the work of the Centre for Rapid and Sustainable Product Development (CDRSP), Marinha Grande, Portugal, for the production of the prototypes, materials and manpower availability.

References

[1] Carvalho, S. S. et al., "Exploring Design Approaches for 3D Printed Antennas," *IEEE Access*, 2024.

[2] Patil, D. D. et al., "3-D-Printed Dual-Band Rectenna System for Green IoT Application," *IEEE Transactions on Circuits and Systems II: Express Briefs*, vol. 70, no. 8, pp. 2864–2868, 2023.

[3] Lira-Valdés, T. et al., "3-D-Printed Spiral Leaky Wave Antenna With Circular Polarization," *IEEE Open Journal of Antennas and Propagation*, vol. 4, pp. 427–433, 2023.

[4] Wu, G.-B. et al., "3-D Printed Circularly Polarized Modified Fresnel Lens Operating at Terahertz Frequencies," *IEEE Transactions on Antennas and Propagation*, vol. 67, no. 7, pp. 4429–4437, 2019.

[5] Nie, B. et al., "A 3D-Printed Subterahertz Metallic Surface-Wave Luneburg Lens Multibeam Antenna," *IEEE Transactions on Terahertz Science and Technology*, vol. 13, no. 3, pp. 297–301, 2023.

[6] Qian, J. et al., "Heatsink Antenna Array for Millimeter-Wave Applications," *IEEE Transactions on Antennas and Propagation*, vol. 68, no. 11, pp. 7664–7669, 2020.

[7] Bi, Y. et al., "3-D Printed Wideband Cassegrain Antenna With a Concave Subreflector for 5G Millimeter-Wave 2-D Multibeam Applications," *IEEE Transactions on Antennas and Propagation*, vol. 68, no. 6, pp. 4362–4371, 2020.

[8] BASF, "Technical Data Sheet - Ultrafuse 316LX," Aug. 2018.

[9] Formfutura, "Technical Data Sheet - MetalFil - Classic Copper," Jul. 2016.

[10] Pellegrini, A. et al., "Evaluation of anisotropic mechanical behaviour of 316L parts realized by metal fused filament fabrication using digital image correlation," *The International Journal of Advanced Manufacturing Technology*, vol. 120, no. 11, pp. 7951–7965, Jun 2022.

[11] Tosto, C. et al., "Fused Deposition Modeling Parameter Optimization for Cost-Effective Metal Part Printing," *Polymers*, vol. 14, no. 16, 2022.

[12] Boschetto, A. et al., "Roughness investigation of steel 316L parts fabricated by Metal Fused Filament Fabrication," *Journal of Manufacturing Processes*, vol. 81, pp. 261–280, 2022.

[13] Rafael, R. et al., "Copper Composites and Laser Sintering: Novel Hybridization Method for 3D Printed Electronics," *Advanced Materials Technologies*, vol. 8, no. 11, p. 2201900, 2023.

[14] Ibrahim, K. A. et al., "Electrical conductivity and porosity in stainless steel 316L scaffolds for electrochemical devices fabricated using selective laser sintering," *Materials & Design*, vol. 106, pp. 51–59, 2016.

[15] Kruželák, J. et al., "Progress in polymers and polymer composites used as efficient materials for EMI shielding," *Nanoscale Advances*, vol. 3, 01 2021.